Jan 1st, 2:30 PM

Determination of Scale Effects for a Scaled Physical Model of a Labyrinth Weir Using CFD

Caterina Torres
University of Leeds, caterina.torres.m@gmail.com

Duncan Borman
University of Leeds

Andy Sleigh
University of Leeds

David Neeve
Arup

Recommended Citation

Torres, Caterina. (2018). Determination of Scale Effects for a Scaled Physical Model of a Labyrinth Weir Using CFD. Daniel Bung, Blake Tullis, 7th IAHR International Symposium on Hydraulic Structures, Aachen, Germany, 15-18 May. doi: 10.15142/T38W7F (978-0-692-13277-7).

7th International Symposium on Hydraulic Structures Aachen, Germany, 15-18 May 2018
ISBN: 978-0-692-13277-7 DOI: 10.15142/T38W7F

Determination of Scale Effects for a Scaled Physical Model of a Labyrinth Weir using CFD

C. Torres[1], D. Borman[2], A. Sleigh[3] & D. Neeve[4]
[1,2,3] *School of Civil Engineering, University of Leeds, Leeds, UK*
[4]*Arup, Leeds, UK*
E-mail: cnctmo@leeds.ac.uk

Abstract: *In the present study the three dimensional (3D) Computational Fluid Dynamics (CFD) Volume of Fluid (VOF) is employed to reproduce the complex hydraulic flows over a labyrinth weir and a spillway for two flow rates, 40 m^3/s and the Probable Maximum Flood (PMF) event of the scheme, 159.5 m^3/s. The VOF method is implemented in two solvers: the open source platform OpenFOAM and the commercial CFD package ANSYS Fluent. Validation is undertaken by modelling the scaled physical model of the scheme. Prototype scale simulations of the two flow rates are conducted, and comparisons between predictions at the two scales are made. Overall the two solvers predict the prototype flows to be shallower and with higher velocities than those at model scale, but with these scale effects becoming less prominent for increasing flow rates. In the 40 m^3/s case the wave structures in the prototype present elongation compared to those at model scale. In the PMF case, the elongation also causes the wave structures to change in position further downstream of the channel. Work is currently underway with the modelling of further flow rates in order to investigate the discrepancies between scale and prototype simulations with increased detail and determine limits to minimise impact of scaling.*

Keywords: *CFD VOF, free surface flows, labyrinth weir, scale effects, scaled physical model.*

1. Introduction

Changes in climate and associated extreme weather episodes are resulting in flood events occurring with higher frequency and severity (Bruwier et al. 2015; Fowler and Kilsby 2003; Kvočka et al. 2016). With predictions of increasing occurrences in the near future, the design and upgrade of existing hydraulic infrastructure such as weirs and spillways is of utmost importance. This type of hydraulic structure plays an essential role in ensuring security of human life as well as safety for developed areas and the natural environment. In particular, labyrinth weirs have been increasingly proposed in recent years, especially in reservoir rehabilitation schemes, given their high efficiency (Paxson and Savage 2006; Tullis et al. 1995). These weirs enable increased storage and discharge without compromising the stability of the dam and hence present resourceful solutions where refurbishment operations are needed due to increased discharge (Lopes et al. 2006; Savage et al. 2004). The typical hydraulic modelling approach for the design of such infrastructure consists of the construction of a scaled physical hydraulic model. These models are scaled representations of a real flow situation (Chanson 2004a). In recent years, instrumentation has developed and hydraulic models allow the simulation of complex phenomena and scenarios with full control of the required modelling conditions (Frostick et al. 2011). For the design of a physical hydraulic model, there is the need to establish similarity between the model and the prototype. A physical model would be identical to the prototype if there is geometrical, kinematic, and dynamic similarity between prototype and model (Chanson 2004b), which is referred to as *mechanical* similarity (Heller 2011; Novak et al. 2010). It is not possible to achieve mechanical similarity with a scaled physical hydraulic model (and same working fluid), and hence the most relevant force ratio is selected and matched in the prototype and model. In hydraulic free surface flows, gravity effects are highly relevant and hence the Froude number similarity is typically chosen. This can lead to the appearance of scale effects due to other force ratios having discrepancies between model and prototype (Chanson 2008). The consequence is that the turbulence levels in the physical model can be significantly lower than in the prototype, and the viscosity and surface tension forces are overestimated, which can have a significant impact on phenomena such as air entrainment (Chanson 2009a). Scale effects due to Froude number similarity have been investigated in several cases in the literature and limits on Reynolds number, Weber number, or water head over weir crest have been established to model several phenomena so that the impact of these effects are minimised. Many examples may be found in Heller et al. (2007), Pfister and Chanson (2012), Pfister et al. (2013), Erpicum et al. (2013), and Erpicum et al. (2016).

The availability of higher computational processing power in the recent decades has enabled the development of several Computational Fluid Dynamics (CFD) approaches to model complex free surface flows. Results from numerical models are able to provide the mapping of the field quantities across the entire modelling domain. One of

the most well-known CFD approaches to simulate free surface hydraulic flows is the Volume of Fluid (VOF) by Hirt and Nichols (1981). The VOF uses a volume fraction function and solves its transport equation in order to locate the interface within a cell. The VOF has been validated to reproduce experimental and real free surface flows in various occasions; some examples can be found in Oertel and Bung (2012), Borman et al. (2014), or Bayon et al. (2016). Labyrinth weirs have been simulated numerically with the VOF method in a number of studies; these include for example, Savage et al. (2004), Paxson and Savage (2006), Crookston et al. (2012), or Savage et al. (2016). CFD models are capable of simulating the flow situation at prototype scale, which is not possible with physical models. Therefore, there is the possibility to quantify scale effects of a scaled physical model once the numerical models are validated by simulating the prototype scale.

The objective of this study is to first simulate a physical scale model of a labyrinth weir and spillway to validate two CFD solvers and then simulate the prototype scale to determine the scale effects of the physical model. The sensitivity of the scale effects to the flow rate is investigated by simulating two flow rates.

2. Description of the Case of Study

The hydraulic structure on which this study focuses consists of a flood storage reservoir, which was built as part of a flood alleviation scheme, comprising an embankment dam, a labyrinth weir and a spillway. The scheme is designed to provide protection for a 1 in 100-year flooding event. The layout of the scheme and a photograph of the physical model are shown in Figure 1. The spillway channel has a length of approximately 150 m from the labyrinth weir to the stilling basin. At the top of the spillway, the labyrinth weir stretches across the full 32 m width of the channel, which is the widest part of the spillway. The labyrinth has a depth of 5.1 m with 4 cycles. 75 m downstream of the weir, the spillway channel narrows to 20 m wide and increases in gradient. 9 m further downstream there is a second change in gradient as the spillway channel becomes gentler and constant until it merges with the stilling basin, which has a horizontal bed. Therefore, the spillway has four different gradients along the channel.

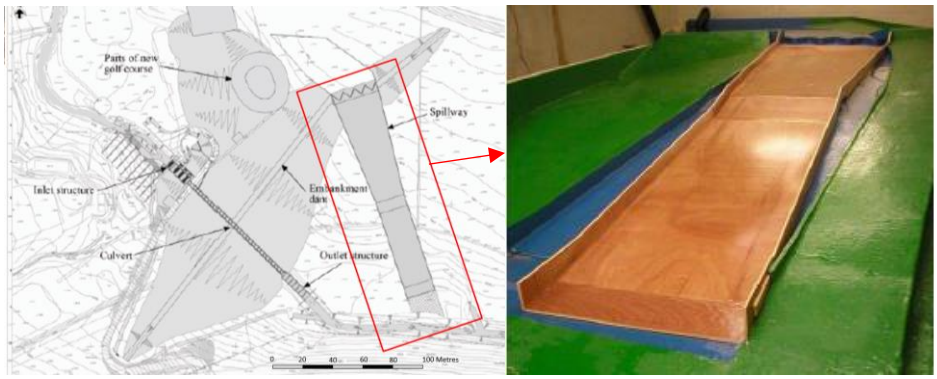

Figure 1. Layout of the hydraulic structures including the embankment dam, the labyrinth weir, and the spillway from Brinded (2014) and physical model.

3. Scaled Physical Hydraulic Model

In order to confirm that the hydraulic structures meet design criteria and to allow inspection of the hydraulic characteristics of the flow, hydraulic modelling was undertaken. A 1:25 scale physical model was commissioned as described in Brinded (2014) with Froude number similarity, where the flow boundary conditions in the model are accordingly scaled to match the Froude number in the prototype and in the physical model. The Froude number is the ratio of inertial force to gravity force, and its expression is outlined in Eq. (1), where v is the velocity, g is the acceleration of gravity, and h is the water depth.

$$Fr = \frac{v}{(gh)^{1/2}} \tag{1}$$

The scale factor of the model is therefore 25 and by geometric similitude, the length ratio is equal to the model geometric scale factor λ, as indicated in Eq. (2) where L_m is the characteristic length in the model and L_p is that in the prototype. Eq. (3) presents the velocity equivalence, where v_m is the water velocity in the model and v_p is the

equivalent in the prototype. The correlation of the flow rate in the model Q_m and in the prototype Q_p is defined in Eq. (4). The time equivalence is indicated in Eq. (5), where T_m is the time in the model and $T_p$is the real time.

$$\lambda = \frac{L_p}{L_m} \tag{2}$$

$$v_p = v_m\sqrt{\lambda} \tag{3}$$

$$Q_p = Q_m\lambda^{5/2} \tag{4}$$

$$T_p = T_m\sqrt{\lambda} \tag{5}$$

4. Numerical Model

4.1. Modelling Domain and Mesh

The three-dimensional layout of the structures with their surroundings was available in CAD drawings. A 3D geometry element comprising the labyrinth weir and the spillway was extracted and the modelling domain was constructed and meshed appropriately. Figure 2(a) presents the outline of the modelling domain for this study, which consists of the approach channel, the labyrinth weir, and the spillway channel. This geometry enables the execution of model validation with physical model measurements of water depth and velocity as well as with observations of the wave structures at a reduced computational cost. The inlet was located at the right side of the spillway upstream the labyrinth weir, as applied in the laboratory, and the inflow boundary condition with constant velocity was invoked. No-slip boundary conditions were applied on the walls and the base of the spillway channel, which included the weir structure. The upper boundary of the computational domain, which in the physical domain is the open air, was defined as atmospheric pressure. For the stilling area a box was designed to simulate flow with the model outlet placed in the left wall of the box with pressure outlet boundary conditions. Simulations were initiated with a constant flow rate at the inlet (equivalent to 40 m^3/s or 159.5 m^3/s). On the scaled simulations the flow rate was scaled according to Eq. (3) in each case. No additional wall roughness was included in the model as the wall characteristics of both scale and prototype (smooth plastic and concrete, respectively) do not indicate this would be necessary. Once validation was complete the prototype structure was modelled using the real size and flow rates.

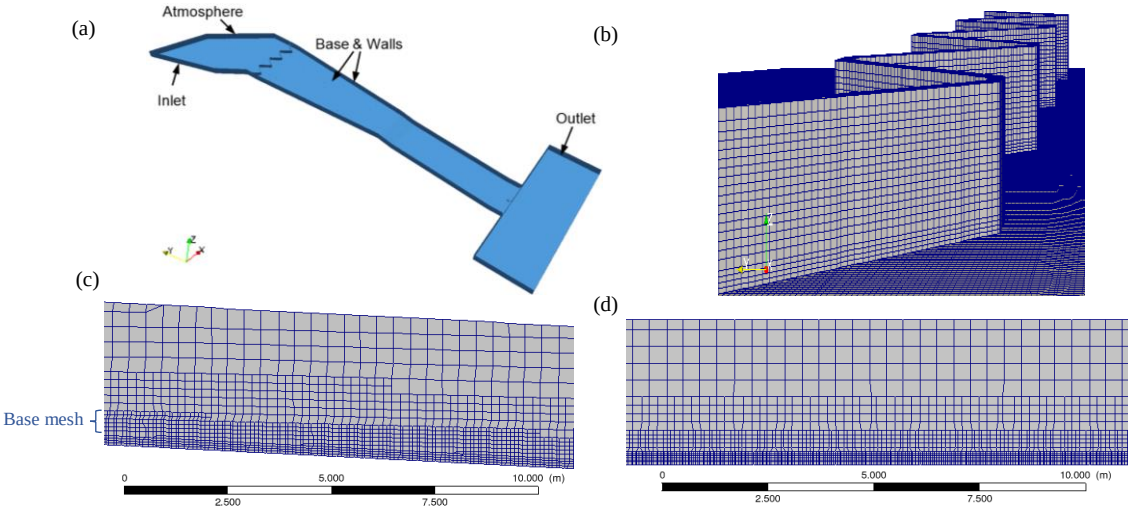

Figure 2. (a): Modelling domain with boundary conditions; (b) Mesh configuration at the labyrinth weir, (c) Longitudinal mesh section at the spillway channel parallel to flow direction; (d) Mesh cross-section of spillway channel in the direction normal to the flow.

In addition to a comprehensive mesh and time-step independence study previously conducted on a simplified geometry detailed in Torres et al. (2017), a mesh convergence study was performed using 3 structured hexahedral meshes with increasing numbers of grid cells. These meshes had 0.6, 2.9, and 7.9 million elements, with base mesh cell sizes at the

area where the free surface is located of 0.5 m, 0.2 m and 0.1 m respectively at the prototype scale. The base cell sizes in the water depth direction were approximately halved at the bed of the spillway where there is an inflation layer. The cell sizes are larger at the atmosphere to optimise the computational effort. The meshes were sized appropriately to represent the scaled physical model, becoming of base cell size 0.02 m, 0.008 m and 0.004 m. Figure 2 (b), (c), and (d) show the configuration of the mesh with highest resolution at the labyrinth weir, at the spillway channel in the direction parallel to the flow, and normal to the flow, respectively. The mesh accuracy was assessed by implementing the Grid Convergence Index (GCI) method specified by the ASME in Celik et al. (2008) at both scales with the two solvers. The variables utilised for the study are velocities and depths at sections A, B, C, D and E as indicated in the diagram of Fig. 5 (c). The mesh refinement ratios r_{12} and r_{23} are 2 and 2.5, both above the recommended minimum of 1.3 by Celik et al. (2008). The mesh independence study revealed that the OpenFOAM simulations were more sensitive to changes of mesh size than those of Fluent. The Fluent simulations presented negligible changes between the predictions of the finest and intermediate meshes and hence the latter was chosen for the Fluent simulations. The GCI values of velocities and depths of the mesh of intermediate resolution were satisfactorily low in Fluent, ranging between 0.1 and 7.6 %. The OpenFOAM GCI values for the intermediate mesh were slightly higher, and the finest mesh was the chosen for the simulations of this solver, with GCI values for depths and velocities between 0.1 and 7 %. CGI values obtained for both solvers at the prototype scale were between 1 and 11 % for the mesh of intermediate resolution, indicating OpenFOAM exhibits lower mesh dependency at the prototype scale. The meshes of intermediate resolution were chosen for the prototype scale simulations in both solvers.

4.2. Numerical Implementations

Scaled and prototype simulations were conducted using a collocated Finite Volume Model (FVM) discretisation on hexahedral cells and the VOF approach for multiphase modelling. Two well-known solvers were utilised to perform the numerical simulations to allow for performance comparison. These are the open source platform OpenFOAM 3.0.1 (Greenshields 2017) and the commercial CFD solver ANSYS Fluent 14.5. (ANSYS 2017). The three-dimensional turbulent nature of the flow in this case required solving the three-dimensional Reynolds Averaged Navier-Stokes (RANS) equations, comprising conservation of mass for an incompressible flow. The standard k-ε model was implemented for closure of the RANS equations, which requires moderate computational resources and presents an appropriate compromise between numerical effort and computational accuracy. This model was chosen after a sensitivity analysis was conducted in respect to the turbulence model, which included the RANS k-ε RNG and the k-ω SST models. The near-wall flow region was modelled with standard wall functions. The free surface was resolved with the VOF method. The VOF solves only one set of equations within the domain and the values of density and dynamic viscosity at the interface are computed by using the values of α at the interface. The interface capturing scheme employed in Fluent is a geometrical reconstruction approach based on the Piecewise Linear Interface Calculation (PLIC), originally proposed by Youngs (1982). In OpenFOAM the corresponding algorithm utilised is an algebraic reconstruction scheme MULES (Multidimensional Universal Limiter for Explicit Solution) (Greenshields 2017), which ensures boundedness and consistency. The VOF method is able to provide a sharp interface between water and air where the volume fraction function value is equal to 0.5, and both phases are allowed to coexist and mix within the same cell. No additional equations are implemented to model the aeration phenomena smaller than the mesh cell size.

5. Validation

Two scaled flow rates were simulated: 40 m^3/s and the PMF of the site which is 159.5 m^3/s. Photographs of the physical model free surface and detailed representations of flow features were available in addition to several measurements of flow depth and velocity at different locations within the spillway channel. These are indicated in the physical model diagrams on Figure 3 (f) and Figure 4 (f). The reported values were the maximum recorded unless the experimental depths fluctuated. Fluctuation depths occur for the PMF case and are indicated on the physical model diagram. The measurement accuracy of depths and velocities of the physical model at the prototype scale is not higher than 25 mm and 0.05 m/s respectively. By extracting time series point data from the numerical simulation, it was observed that steady state occurred after approximately 90 s of simulated real flow time. Results presented here are all time-averaged predictions extracted from the simulation at times between 100 and 130 s, when the monitored predictions had remained stable for a minimum of 10 s and generally within a time window of 30 s. Within such time window the variation in the results was minimal with a standard deviation of typically around 0.001.

Figure 3 (a) shows the complex configuration of cross-waves generated by the labyrinth weir in the physical model and predicted with the two solvers for 40 m^3/s. All of the cross-waves observed in the physical model photographs and indicated in the model diagram are well predicted by the two numerical codes. The numerical predictions were extracted at locations in the vicinity of the measurement locations informed by their position in the physical model diagram. It is estimated that the maximum difference in x and y between the location of the measurement point and the location where numerical data is extracted is approximately 0.01 m in the physical model, which is equivalent to 0.25 m in the prototype. Figure 3 (b) shows the water free surface coloured by velocity magnitude with the location where the data for measurement point A was extracted. The contours of the water volume fraction on a plane through location A are shown with a line indicating the location of the point. A graph of the free surface depths and features at this plane is presented on Figure 3 (c). The free surface features are very accurately represented along the section and the depth predictions show good agreement with the experimental measurement at this location. Figure 3 (d) shows the velocity cross-sectional profiles at sections B, C, D, and E of the spillway channel. The results from both solvers are very comparable across all sections of the spillway channel, with velocity values being only slightly higher in the Fluent predictions across-section C. Figure 3 (e) shows the single point predictions extracted at the several experimental locations. Such predictions show good agreement with the experimental measurements and consistency between the two solvers. Figure 3 (f) shows the physical model diagram with the location of all measurement points and the configuration of the cross-waves' crests.

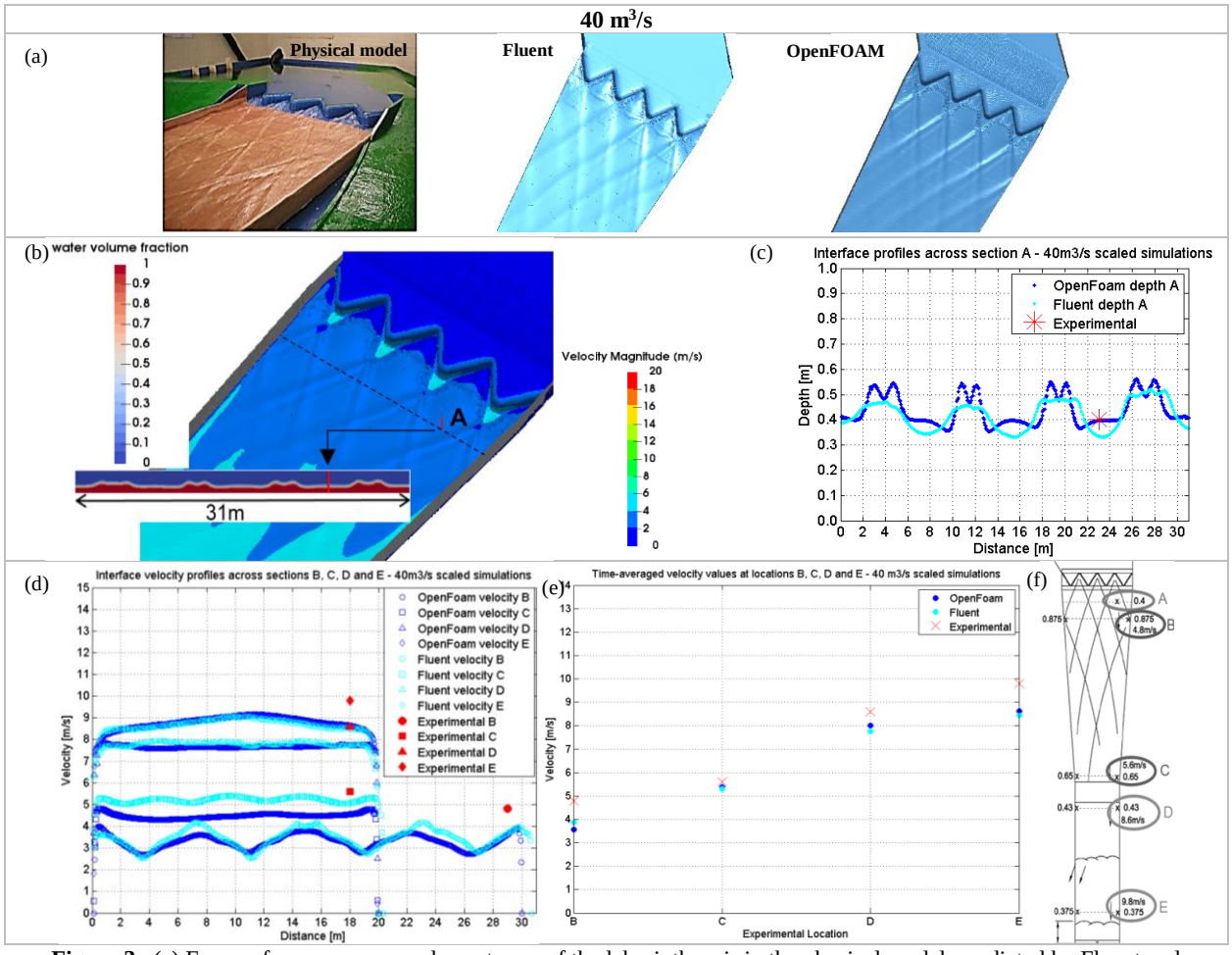

Figure 3. (a) Free surface cross waves downstream of the labyrinth weir in the physical model, predicted by Fluent and OpenFOAM; (b) Velocity-coloured free surface with a water volume fraction contours plane through point A; (c) Free surface profile at a section across point A; (d) Free surface velocity profiles at sections through points B, C, D, and E; (e) Velocity values at the measurement point locations; (f) Physical model diagram.

Figure 4 (a) shows the physical model free surface patterns, and predicted with the two solvers for the PMF case. In this flow rate, all the cross-wave crests observed in the physical model are also predicted numerically. However, the

predictions from the two solvers exhibit increased differences than for the 40 m^3/s case, with the Fluent cross-waves demonstrating greater prominence than those predicted in OpenFOAM. In order to investigate such differences, an additional simulation was conducted using the Compressive Interface Capturing Scheme for Arbitrary Meshes scheme (CICSAM) in Fluent, which is an algebraic interface reconstruction scheme, more similar to that implemented in OpenFOAM. Results from simulations using the CICSAM in Fluent presented higher resemblance to the OpenFOAM predictions with lower depths. Therefore, the interface capturing scheme is believed to be one of the main causes of the variation in the free surface predictions of the two solvers. Figure 4 (b) shows the cross-sectional profiles of depth at sections A and B and the depths at point locations A to E are presented on Figure 4 (c). The largest discrepancies between the water depth point data predictions and the physical model measurements are at location B, although the numerical predictions present a fluctuation range of approximately 0.2 m at locations A to C. Overall, the Fluent predictions are in good agreement for the rest of the points of the spillway channel, but the OpenFOAM predictions exhibit an underestimation of the free surface depth in most cases. Figure 4 (d) shows the time series velocity magnitude values at the free surface extracted at point locations B to E predicted with Fluent. Figure 4 (e) indicates the surface velocity profiles at various sections of the spillway. The greatest difference between numerical and experimental velocity values occurs at point D, but overall, such plots confirm that the free surface velocities predicted by Fluent are in good agreement with the physical model measurements. The velocity predictions from OpenFOAM at D and E appear to be slightly lower than the physical model measurements.

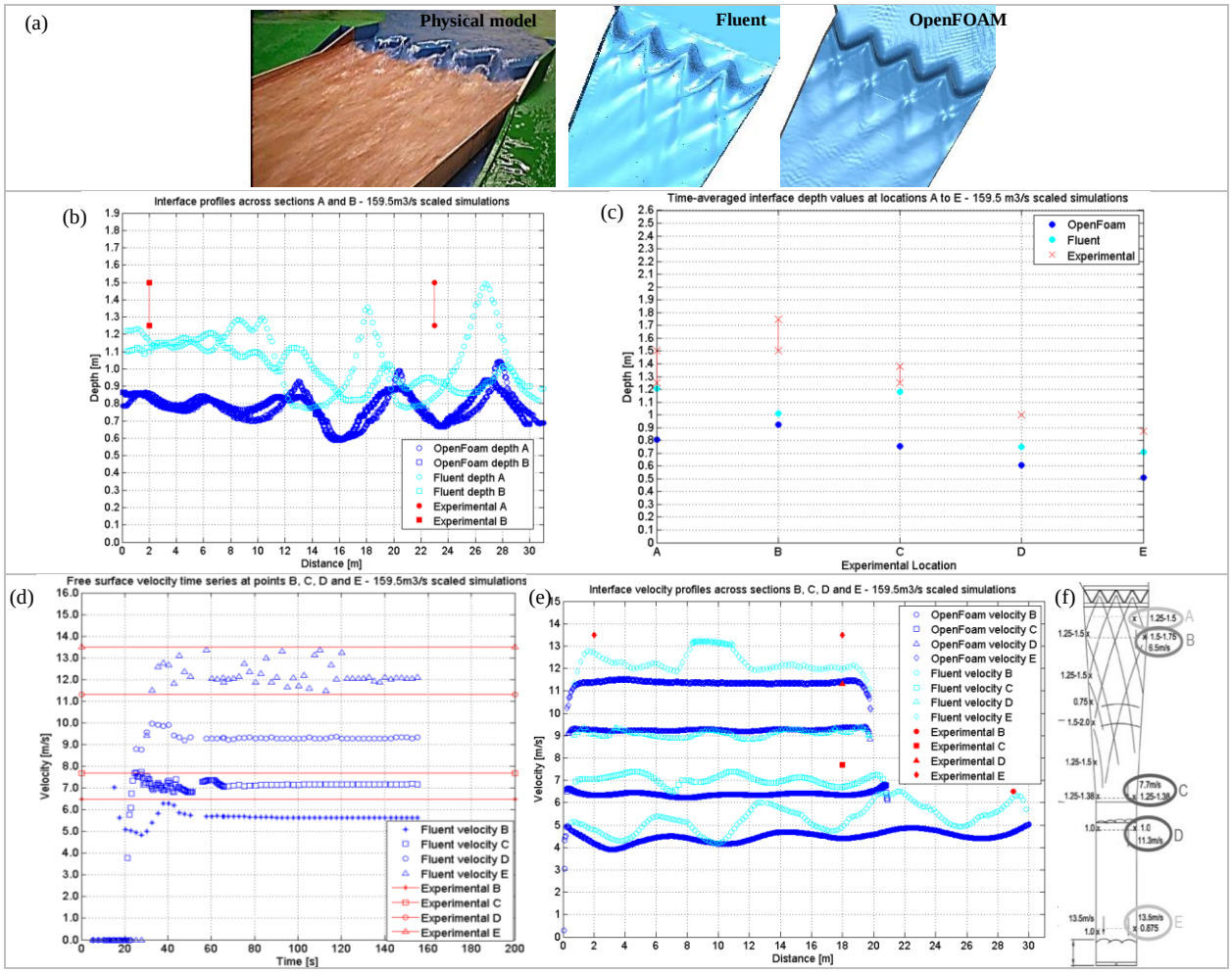

Figure 4. (a) Free surface cross-waves downstream of the labyrinth weir in the physical model, predicted by Fluent and OpenFOAM; (b) Cross-sectional profiles of free surface depth through points A and B; (c) Free surface depth values at point locations A to E; (d) Velocity time series point locations B to E from t= 0 s to steady state; (e) free surface velocity profiles through points B, C, D, and E of the spillway channel; (f) diagram of experimental measurements for 159.5 m^3/s.

6. Simulating Prototype Scale and Comparison with Model Scale Predictions

6.1. Depths and Velocities

Prototype scale simulations of the 40 m^3/s and PMF flow rates were conducted and differences in the flow characteristics at the two scales were analysed. Results from the two solvers consistently show there is an increase in velocity and a decrease in depth in the prototype compared to the scaled predictions.

In order to examine the decrease in depth and increase in velocity observed at prototype scale, the water depths and velocities at the two scales were extracted and averaged across a number of sections of the spillway channel. Table 1 shows the percentage difference in the prototype values with respect to those at the model scale at four sections. The percentage difference in water depths at sections B, C, D, and E correspond to dh_B, dh_C, dh_D, and dh_E respectively. The velocity percentage differences are dv_B, dv_C, dv_D, and dv_E respectively. In Table 1 it is observed that the decrease in water depth and the increase in velocity in the prototype predicted by the two solvers is consistently larger for the 40 m^3/s case than for the 159.5 m^3/s in all sections.

Table 1. Percentage difference in depth and velocity of prototype with respect to model predictions at sections B, C, D, and E.

	Q [m^3/s]	dh_B [%]	dh_C [%]	dh_D [%]	dh_E [%]	dv_B [%]	dv_C [%]	dv_D [%]	dv_E [%]
OpenFOAM	40	-15.1	-18.6	-16.4	-15.9	18.4	23.5	7.1	7.5
OpenFOAM	159.5	-9.0	-2.7	-0.4	-0.9	13.7	10.8	3.0	5.8
Fluent	40	-12.8	-14.6	-11	-19.6	12.7	14.3	3.1	19.8
Fluent	159.5	-5.7	-12.8	-6.3	-5.6	3.6	4.8	3.0	3.7

6.2. Wave Features

Figure 5 (a) details the configuration of the cross-wave crests for the 40 m^3/s scaled and prototype cases. It is observed that there are significant changes in the prototype compared to the scaled case. The cross-waves' crests configuration becomes elongated, and therefore, the waves' crests crossing points in the prototype are located further downstream than in the scaled case. In order to quantify the level of stretching of the cross-waves, the plan view distance between three waves' crossing points and the weir downstream crest were measured. The three distances measured, x_1, x_2, and x_3 are indicated on Figure 5 (a). On average in the 40 m^3/s flow rate, the wave structures in the prototype are approximately between 2 and 16 % elongated in respect to the scaled ones. In the 159.5 m^3/s case the stretching of the waves is approximately of 11 to 14 %. Figure 5 (b) shows the OpenFOAM and Fluent predictions of free surface depth at sections C, D, and E of the spillway channel for the scaled and prototype simulations. The free surface profiles reveal that as a consequence of the changes in the cross-wave configuration of larger waves, the free surface features downstream of the channel also present greater differences in the two scales. The elongation of the cross-waves in the prototype causes the impact point from the wave generated in the first weir bay to be located further downstream than that in the scaled case. This makes the reflective wave to cross the channel from left to right further downstream. At section D (located immediately after the spillway second change in gradient), the prototype simulations show the wave shifted towards the left side of the channel while the scaled case shows a central wave. This situation is captured by the two solvers. The central wave in the scaled simulations is reproduced in the physical model and occurs because the impact point is further upstream. The crest of the shifted and central cross-waves and the location of the impact points denoted with "I" at the two scales are indicated on Figure 5 (c). A further view of the difference in the waves' configurations is presented on Figure 5 (d). The waves generated downstream of the second change in gradient in the physical scale model appear to agree with the scaled simulation predictions, and the prototype predictions exhibit the shifted position of the dominant wave crest.

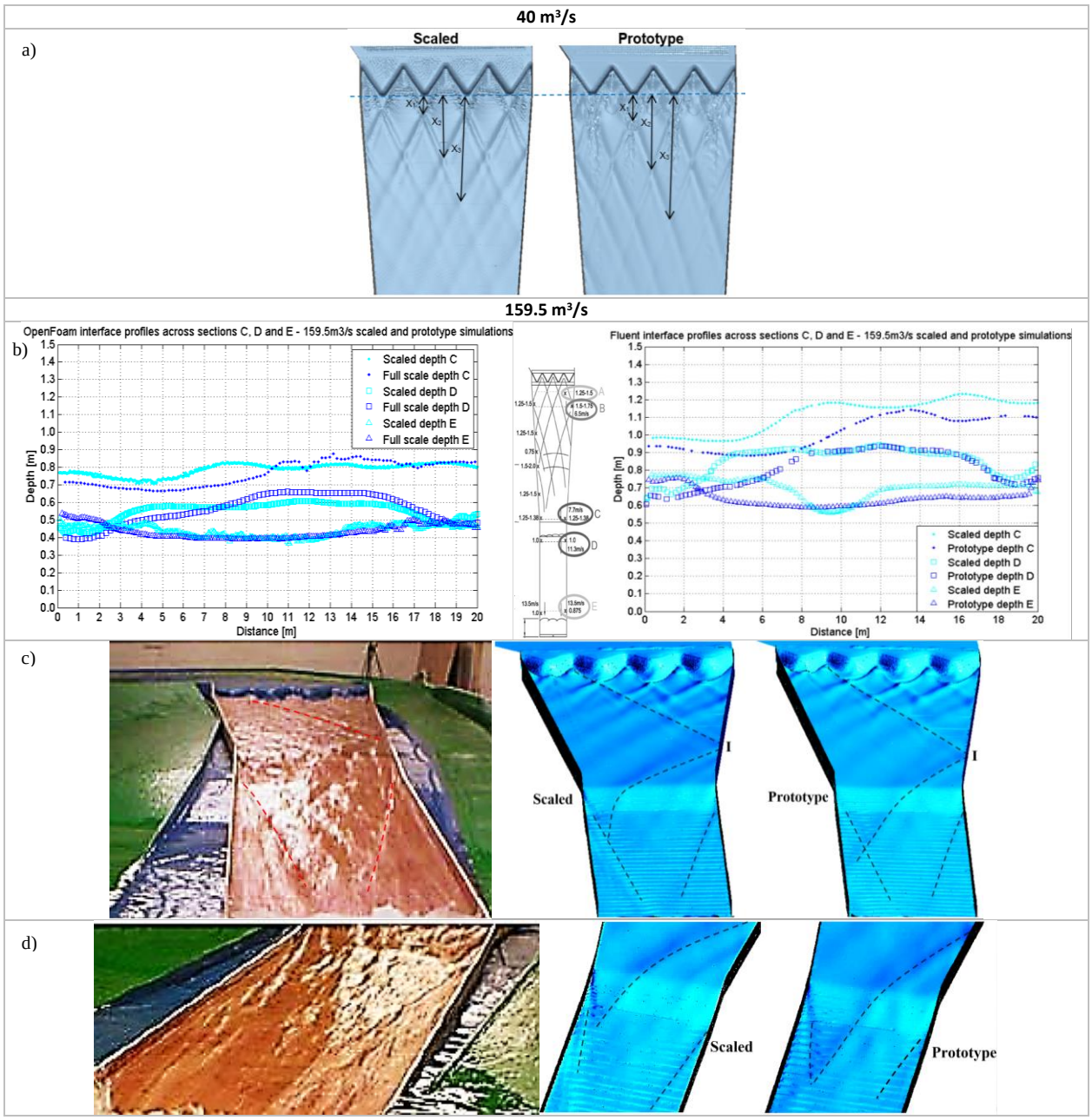

Figure 5. **(**a) 40 m^3/s Free surface cross-waves' crests with measurement arrows to crossing points in scaled and prototype simulations; (b) 159.5 m^3/s cross-sectional profiles of free surface depth at sections through C, D, and E for the scaled and prototype cases predicted with OpenFOAM and Fluent; (c) Free surface cross-waves and main features at the physical model and predicted with Fluent for the scaled and prototype cases; (d) Physical model and numerical predictions of the waves downstream second change in gradient.

6.3. Discussion

Results show that overall, the difference in depths and velocities is most significant for the lower flow rate. This is in line with theory, since low depths and velocities in scaled flows are most likely to be impacted by scaling assumptions. This is typically due to the overestimation of the viscous and surface tension forces in Froude similarity models, which in such case become non-negligible forces. This has been reported in the literature in a number of cases (Chanson 2009b; Novak et al. 2010; Pfister et al. 2013). For higher depths and velocities, the effects of these forces decrease and so does the impact of scaling (Heller 2011). The decrease in depth for the two solvers is predicted to be approximately between 14 to 18 % in the 40 m^3/s case and 4 to 6 % in the 159.5m^3/s case. The increase in velocity

has a similar trend, which indicates an increase of around 12 to 14 % in the 40 m^3/s case and of 4 to 8 % in the 159.5m^3/s case. These percentages have been calculated by averaging the percentage difference at sections A, B, C, D, and E, and these are representative values of the general variations along the spillway channel.

Although the largest flow rate shows the lowest scale effects in depth and velocity predictions, the PMF shows more significant variations in the configuration and shape of the wave structures. This suggests that these wave features, which are of significant interest to practitioners and designers, are the challenging aspect to predict accurately within the physical model scale. Further simulations of a wider range of flow rates and scales are currently being undertaken and will be presented in the Symposium. Such results will allow the derivation of more specific limits that would minimise scale effects on wave features for this particular structure.

7. Conclusions

In this work, 3D CFD VOF simulations of hydraulic flows over a prototype labyrinth weir and spillway were conducted using the ANSYS Fluent and OpenFOAM solvers. Numerical simulations of the physical scale model were first undertaken in order to validate the models for two flow rates: 40 m^3/s and the PMF of the site 159.5 m^3/s. For the 40 m^3/s case the two solvers present good agreement with the physical model measurements and consistency in their predictions. For the PMF the Fluent predictions demonstrate closer agreement with the physical model than those from OpenFOAM, which appear to be slightly underestimating water depths and in some sections the velocity. Once validation was completed, prototype simulations were performed for the equivalent real size flow rates. The comparison between scaled and prototype predictions for both solvers shows the prototype flows exhibit lower free surface depths and higher velocities. The depth discrepancies between scaled and prototype flows are larger for the lowest flow rate, being of approximately 16 % for 40 m^3/s and of 5 % for the PMF. The increase in velocity also reduces for increasing flow rate, with a difference of approximately 13 % for the 40 m^3/s case and about 6 % in the PMF. In addition, the prototype wave structures present elongation in both flow rates, which in the PMF also causes a change in position of the wave features downstream the spillway channel. The free surface features and patterns are therefore a complex aspect to predict with physical models given the existing challenges to scale these up. This could have implications on the design of hydraulic structures where wave features are of critical importance since this study shows they may not be reproduced in the same way in the prototype. Further investigations are currently being undertaken in order to determine limits to minimise scale effects for this structure with numerical simulations of a wider range of flow rates and scales.

8. Acknowledgements

This work was supported by the Engineering and Physical Sciences Research Council (EPSRC) in conjunction with Arup Leeds.

9. References

ANSYS, I. (2017). *ANSYS Fluent.* [Online]. [Accessed 07/08/2017]. Available from: http://www.ansys.com/Products/Fluids/ANSYS-Fluent.

Bayon, A., Valero, D., García-Bartual, R., Vallés-Morán, F. J. and López-Jiménez, P. A. 2016. "Performance assessment of OpenFOAM and FLOW-3D in the numerical modeling of a low Reynolds number hydraulic jump." *Environmental Modelling & Software,* 80, 322-335.

Borman, D., Sleigh, A., Coughtrie, A. and Horton, L. 2014. "Hydraulic free surface modelling with a novel validation approach." *9th South African Conference on Computational and Applied Mechanics, Somerset West*.

Brinded, P., Gilbert, R., Kelham, P., and Peters, A. 2014. "Eller Beck Flood Storage Reservoir – the challenges of low impact flood storage design." *18th Biennial Conference of the British Dam Society at Queen's University, Belfast*. ICE Publishing.

Bruwier, M., Erpicum, S., Pirotton, M., Archambeau, P. and Dewals, B. J. 2015. "Assessing the operation rules of a reservoir system based on a detailed modelling chain." *Natural Hazards and Earth System Science*, 15(3), 365-379.

Celik, I., B, Ghia, U., Roache, P. J., Freitas, C. J., Coleman, H. and Raad, P. E. 2008. "Procedure for Estimation and Reporting of Uncertainty Due to Discretization in CFD Applications." *Journal of Fluids Engineering*, 130(7), 1-4.

Chanson, H. (2004a). "Air-water flows in water engineering and hydraulic structures. Basic processes and metrology." Yazdandoost, F. and Attari, J. eds. *Hydraulics of Dams and River Structures.* London: Taylor & Francis Group.

Chanson, H. (2004b). *The hydraulics of open channel flow: an introduction; basic principles, sediment motion, hydraulic modelling, design of hydraulic structures.* Oxford [UK]: Elsevier Butterworth Heinemann.

Chanson, H. (2009a). "Current knowledge in hydraulic jumps and related phenomena. A survey of experimental results." *European Journal of Mechanics - B/Fluids,* 28(2), 191-210.

Chanson, H. (2009b). "Turbulent air–water flows in hydraulic structures: dynamic similarity and scale effects." *Environmental Fluid Mechanic*,. 9(2), 125-142.

Crookston, B. M., Paxson, G. S. and Savage, B. M. 2012. "Hydraulic Performance of Labyrinth Weirs for High Headwater Ratios." Matos, J., et al., eds. *4th IAHR International Symposium on Hydraulic Structures 9-11 February 2012, Porto, Portugal*. IAHR.

Erpicum, S., Silvestri, A., Dewals, B., Archambeau, P. and Pirotton, M. 2013. "Escoloubre Piano Key weir: Prototype versus scale models." *Second international workshop on labyrinth and piano key weirs, Chatou, Paris, France*.

Erpicum, S., Tullis, B. P., Lodomez, M., Archambeau, P., Dewals, B. J. and Pirotton, M. "Scale effects in physical piano key weirs models." *Journal of Hydraulic Research.* 54(6), 692-698.

Fowler, H.J., and Kilsby, C.G. (2003). "Implications of changes in seasonal and annual extreme rainfall." *Geophysical Research Letters,* 30(13).

Frostick, L. E., Mclelland, S. J. and (Eds), T. G. M. 2011. *Users Guide to Physical Modelling and Experimentation. Experience of the HYDRALAB Network.* Leiden [The Netherlands].

Greenshields, C.J. (2017). *OpenFOAM: The OpenFOAM Foundation User Guide* OpenFOAM Foundation Ltd.

Heller, V. (2011). "Scale effects in physical hydraulic engineering models." *Journal of Hydraulic Research,* 49(3), 293-306.

Heller, V., Hager, W. H. and Minor, H.-E. 2007. "Scale effects in subaerial landslide generated impulse waves." *Experiments in Fluids.* 44(5), 691-703.

Hirt, C.W., and Nichols, B.D. (1981). "VOF method for the dynamics of free boundaries." *Journal of Computational Physics,* 39, 201-225.

Kvočka, D., Falconer, R. A. and Bray, M. 2016. "Flood hazard assessment for extreme flood events." *Natural Hazards,* 84(3), 1569-1599.

Lopes, R., Matos, J. and J., M. 2006. "Discharge capacity and residual energy of labyrinth weirs." *International Junior Researcher and Engineer Worksop onHydraulic Structures (IJREWHS '06), Brisbane, Australia*. Division of Civil Engineering, Univ. of Queensland, 47-55.

Novak, P., Guinot, V., Jeffrey, A. and Reeve, D. 2010. *Hydraulic Modelling - An Introduction. Principles Methods and Applications.* New York: Spon Press.

Oertel, M., and Bung, D.B. (2012). "Initial stage of two-dimensional dam-break waves: laboratory versus VOF." *Journal of Hydraulic Research,* 50(1), 89-97.

Paxson, G., and Savage, B. (2006). "Labyrinth spillways: Comparison of two popular U.S.A. design methods-and-consideration of non standard approach conditions and geometries." Matos, J. and Chanson, H., eds. *International Junior Researcher and Engineer Workshop on Hydraulic Structures, Brisbane, Australia*. Univ. of Queensland.

Pfister, M., Battisacco, E., De Cesare, G. and Schleiss, A. J. 2013. "Scale effects related to the rating curve of cylindrically crested Piano Key weirs." *Second international workshop on labyrinth and piano key weirs, Chatou, Paris, France*.

Pfister, M., and Chanson, H. (2012). "Discussion of Scale effects in physical hydraulic engineering models." *Journal of Hydraulic Research,* 50(2), 244-246

Savage, B., Crookston, B. and Paxson, G. 2016. "Physical and numerical Modeling of large headwater ratios for a 15 degrees labyrinth spillway." *Journal of Hydraulic Engineering,* 142(11), 1-7.

Savage, B. M., Frizell, K. and Crowder, J. 2004. "Brains versus Brawn. The changing world of hydraulic model studies." *Dam Safety, ASDSO, Lexington, KY*.

Torres, C., Borman, D., Sleigh, A. and Neeve, D. 2017. "Three dimensional numerical modelling of full-scale hydraulic structures." *Proceedings of the 37th IAHR World Congress, Kuala Lumpur, Malaysia*. 1335-1343.

Tullis, J. P., Amanian, N. and Waldron, D. 1995. "Design of Labyrinth Spillways." *Journal of Hydraulic Engineering*, 121(3), 247-255.

Youngs, D.L. (1982). "Time dependent multi material flow with large fluid distortion." *Numerical Methods for Fluid dynamics*, 273-285.